PHYSICAL REVIEW B **89**, 060506(R) (2014)

Interface charge doping effects on superconductivity of single-unit-cell FeSe films on $SrTiO_3$ substrates

Wenhao Zhang,[1,2] Zhi Li,[2] Fangsen Li,[1,2] Huimin Zhang,[2] Junping Peng,[2] Chenjia Tang,[1,2] Qingyan Wang,[1] Ke He,[1,2,3] Xi Chen,[1,3] Lili Wang,[1,2,3,*] Xucun Ma,[1,2,3,†] and Qi-Kun Xue[1,3]

[1]*State Key Laboratory of Low-Dimensional Quantum Physics, Department of Physics, Tsinghua University, Beijing 100084, China*

[2]*Institute of Physics, Chinese Academy of Sciences, Beijing 100190, China*

[3]*Collaborative Innovation Center of Quantum Matter, Beijing, China*

(Received 31 December 2013; revised manuscript received 12 February 2014; published 25 February 2014)

We prepare single-unit-cell FeSe films on insulating $SrTiO_3$ substrates by molecular beam epitaxy and investigate the evolution of their superconducting properties with annealing by *in situ* scanning tunneling microscopy and scanning tunneling spectroscopy and *ex situ* transport measurements. We find that through an annealing process, the superconductivity of 1-uc FeSe films on $SrTiO_3$ substrates develops with the formation of stoichiometric FeSe films and is further enhanced by charge transfer from $SrTiO_3$ substrates to FeSe films. Moreover, the superconductivity is independent of the bulk property of the $SrTiO_3$ substrate, regardless of whether it is insulating or conductive. Our results reveal that the high-temperature superconductivity of 1-uc FeSe films on $SrTiO_3$ substrates indeed occurs at the FeSe/$SrTiO_3$ interface, where the electron doping at FeSe films plays an important role in this interfacial superconductivity.

DOI: 10.1103/PhysRevB.89.060506 PACS number(s): 74.78.−w, 74.25.F−, 74.45.+c, 74.62.Dh

Recently discovered superconductivity in the single-unit-cell (1-uc) FeSe films on Nb-doped $SrTiO_3$ (Nb-STO) substrates has attracted intensive attention [1–8]. In sharp contrast to the results of FeSe films on graphene where a 2.2 meV superconducting gap is observed on thick (30 nm) films and no superconducting gap on 1-uc FeSe down to 2.3 K [2], 1-uc FeSe films on STO substrates exhibit unexpected large superconducting gaps of 15–20 meV. More intriguingly, the anomalously large superconducting gaps are only found in the first uc FeSe but not on 2-uc or thicker layers, indicating that the interface plays an important role in the enhanced superconductivity in 1-uc FeSe films on STO substrates [4,6–8].

Several theoretical scenarios have been proposed to explain the interfacial superconductivity. For example, the soft phonons at the interface can enhance the energy scale of Cooper pairing and even change the pairing symmetry, then increase the superconducting transition temperature (T_C) [9,10]. It is also pointed out that the key factor may be oxygen deficiency, which induces charge transfer and enhances binding energy at the interface [11]. All the previous scanning tunneling microscopy and scanning tunneling spectroscopy (STM/STS) and angle-resolved photoemission spectroscopy (ARPES) studies used Nb-STO as the substrate [4,7,8]. The Nb-STO substrates were pretreated by Se etching, and annealed at 950 °C under Se flux for 30 min in an ultrahigh-vacuum (UHV) chamber [4], which did induce oxygen deficiency [8,12]. Is the Se etching necessary to obtain the high T_C? What happens during annealing? In this Rapid Communication, we investigate the evolution of the morphology and superconducting properties of 1-uc FeSe films on insulating STO substrates with annealing by *in situ* STM and STS and *ex situ* transport measurements. Our study shows that the superconductivity of 1-uc FeSe films on STO substrates occurs only when stoichiometric FeSe is formed and is gradually enhanced by annealing. The superconducting gap is independent of the bulk property, whether it is insulating or conductive, of STO substrates. Our results reveal that the enhanced superconductivity is induced by the interface effect, and electron doping at the FeSe/STO interface plays an important role. Based on the evolution of morphology and carrier concentration with annealing, we discuss the possible origin of electron doping.

The insulating STO substrates were prepared with standard chemical and thermal treatments in a tube furnace to obtain a specific TiO_2-terminated surface [13]. Then, the STO substrates were transferred into the UHV chamber (base pressure 3×10^{-10} mbar) and annealed at 600 °C for 3 h. This treatment introduces a two-dimensional electron gas (2DEG) on the surface, while the STO remains bulk insulating [14]. FeSe films were grown by coevaporating Fe (99.995%) and Se (99.9999%) with a flux ratio of ∼1:10 from two standard Knudsen cells. The STO substrate was held at 400 °C and the growth rate was ∼0.182 uc/min. Under the above growth condition, the FeSe films were macroscopically homogeneous, which is very critical for transport measurements. The as-grown FeSe films were successively annealed in the UHV chamber for several hours at various temperatures ranging from 250 to 550 °C. The STM and STS measurements were performed *in situ* to record the morphology and conductance spectra after each annealing treatment, with all STM images taken at 4.2 K. Additional 10-uc insulating FeTe and ∼30 nm amorphous Si layers were deposited onto 1-uc FeSe films as protection layers for *ex situ* transport measurements. The insulating STO substrate and FeTe capping layer ensure that electrical transport measurements reflect the property of the FeSe/STO films [13]. The transport measurements were performed by using standard six-terminal geometry on a commercial Quantum Design physical property measurement system (PPMS) with a magnetic field up to 9 T.

Figure 1(a) shows a typical large-scale STM image of as-grown 1-uc FeSe films. The as-grown FeSe surface is

*liliwang@mail.tsinghua.edu.cn

†xucunma@mail.tsinghua.edu.cn

 ©2014 American Physical Society

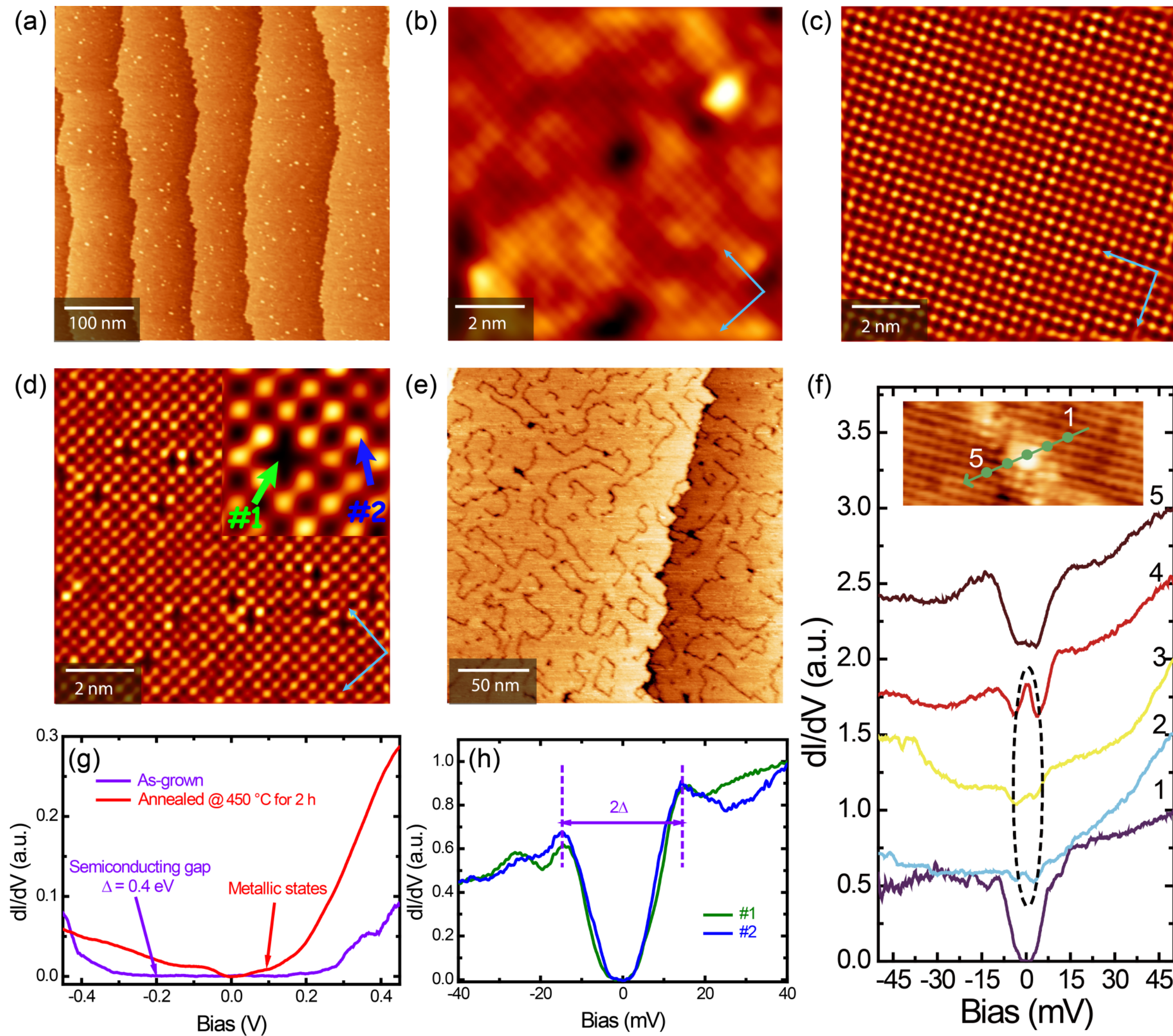

FIG. 1. (Color online) (a) The STM morphology of an as-grown 1-uc FeSe film. (b)–(d) Atomically resolved images after annealing at 400, 450, and 530 °C for 2 h, respectively. (e) The STM morphology of a 1-uc FeSe film annealed at 450 °C for more than 10 h. Tunneling current: 50 pA; sample bias: (a) +2.0 V, (b) +0.5 V, (c) and (d) +1.0 V, and (e) +2.0 V. The blue arrows in (b)–(d) indicate the direction of the in-plane lattice constant. (c) and (d) are filtered by fast Fourier transformation (FFT) using WSxM software. (f) dI/dV spectra taken along the line across the domain wall labeled as blue dots (see the inset). The spectra are shifted along the y axis at a fixed value of 0.5. (g) dI/dV spectra of as-grown 1-uc FeSe films (purple curve) and after annealing at 450 °C for 2 h (red curve). (h) dI/dV spectra taken on No. 1 and No. 2 sites labeled in (d).

atomically flat with regular steps originating from the STO substrate. Extra Se adatoms tend to appear on the surface in the form of bright dots in Fig. 1(a), which is due to the Se-rich growth condition. Figures 1(b)–1(d) are the atomically resolved topographic images after successive annealing at 400, 450, and 530 °C for 2 h in each cycle, respectively. The images of FeSe annealed between 450 and 480 °C are similar to Fig. 1(c), while those from 500 to 530 °C are similar to Fig. 1(d). The Se adatoms decrease in both quantity and size during annealing at 400 °C, while the extra Se adatoms are still visible [bright dots in Fig. 1(b)]. Stoichiometric FeSe is obtained after annealing at 450 °C [Fig. 1(c)]. Se vacancies emerge after annealing at 530 °C [Fig. 1(d)]. All the surfaces shown in Figs. 1(b)–1(d) are Se-terminated squarelike 1×1 with in-plane lattice constants $a = b = 3.8$ Å. Compared with the in-plane lattice constants of 3.77 and 3.91 Å for the bulk FeSe and STO substrate [15], the epitaxial FeSe film experiences a small in-plane tensile stress (lattice distortion <1%). We note that the 1-uc FeSe films on an insulating STO substrate have the same in-plane lattice constants as those on Se-etched STO substrates [4]. However, the 2×1 unidirectional stripe, which was observed on the 1-uc FeSe films on Se-etched STO substrates and revealed to be purely an electronic feature instead of lattice reconstruction [4,16], is not observed here. We also find that the surface morphology remains similar to Fig. 1(c) even after annealing at 450 °C for 30 h, while Se vacancies emerge after annealing at 500 °C for 2 h [Fig. 1(d)]. Annealing above 550 °C causes decomposition of FeSe films (not shown). This implies that 450 °C is the optimal temperature to keep FeSe stoichiometric. So we set the annealing temperature at 450 °C and improve the film morphology for *ex situ* transport measurements by increasing the annealing time. It is worth noting that annealing above 450 °C induces the appearance of domains on the

single-uc FeSe films. Figure 1(e) is the STM morphology after annealing the sample at 450 °C more than 10 h, showing the domain structure on the single-uc FeSe films.

With increasing annealing temperature, the FeSe films change from semiconductive to metallic, and finally reach a superconductive state. Figure 1(g) shows the typical dI/dV spectra taken on as-grown FeSe films and annealed at 400 °C for 2 h. It is clearly seen that the as-grown FeSe film is semiconducting with an energy gap of 0.4 eV (purple curve), while it becomes metallic after annealing (red curve). Figure 2(a) shows a series of spatial averaged tunneling spectra taken after annealing at 450, 480, 500, 510, and 530 °C for 2 h, respectively. These U-shaped dI/dV spectra with pronounced peaks indicate that the films are in the superconducting state. Moreover, the superconducting gap (Δ), defined as half of the energy between two coherent peaks near the Fermi level (E_F), gradually becomes larger with increasing annealing temperature. The gap reaches ~15.4 meV after annealing at 530 °C, roughly agreeing with the gap size of 1-uc FeSe films on Se-etched STO substrates within experimental uncertainties [4,6–8]. Shown in Fig. 2(b) is the detailed gap size evolution on annealing, with the gap size averagely calculated over more than ten points. In Fig. 2(c), we show a series of temperature-dependent normalized tunneling spectra taken on the FeSe surface after annealing at 530 °C. Here all the tunneling spectra were normalized by their backgrounds (presumed to be the normal-state conductance), which was extracted from a cubic fit to the conductance for $|V| > 30$ mV [17]. With increasing temperature, the spectra become broadened and the coherence peaks are gradually suppressed. Meanwhile, the zero bias conductance (ZBC) continuously increases [Fig. 2(d)]. The energy gap is still visible at 50.1 K, suggesting that T_C is higher than this temperature. Near T_C, the ZBC shows a linear dependence on temperature, as shown in Fig. 2(d). By extrapolating T_C to the point where ZBC = 1 [18], we find a $T_C \sim 68$ K for the 1-uc FeSe/STO film, which is also consistent with the value of 65 K in single-uc FeSe films on Se-etched Nb-STO substrates revealed by ARPES [7,8]. The similar results on different substrates further confirm that the high-T_C superconductivity of 1-uc FeSe films on STO substrates is an interfacial effect.

The *ex situ* transport results of the 1-uc FeSe films annealed at 450 °C for various times are shown in Fig. 3. The temperature-dependent resistance $R(T)$ in Fig. 3(a) clearly shows that T_C^{onset} becomes larger with increasing annealing time, where T_C^{onset} is defined as the intersection between the linear extrapolation of the normal state and the superconducting transition. It is worth noting that here the highest T_C^{onset} of 40 K is much lower than that observed by STS above (68 K). We attribute this discrepancy to a possible reason as follows: In *ex situ* transport measurements, FeTe films are grown over the FeSe films as a protection layer, where the magnetic order in FeTe [19] may suppress the superconductivity in the 1-uc FeSe films on STO [13]. In addition, STS measurements are critical and locally sensitive while the transport technique is a macroscopic probe. The current FeSe films consist of domains and defects [Fig. 1(e)]. Impurity-induced bound states are observed on the domain walls [Fig. 1(f)], indicating that superconductivity could be locally suppressed with Josephson junctions and electron scattering [20].

The corresponding Hall coefficient (R_H) in Fig. 3(b) exhibits a systematic evolution with increasing annealing time

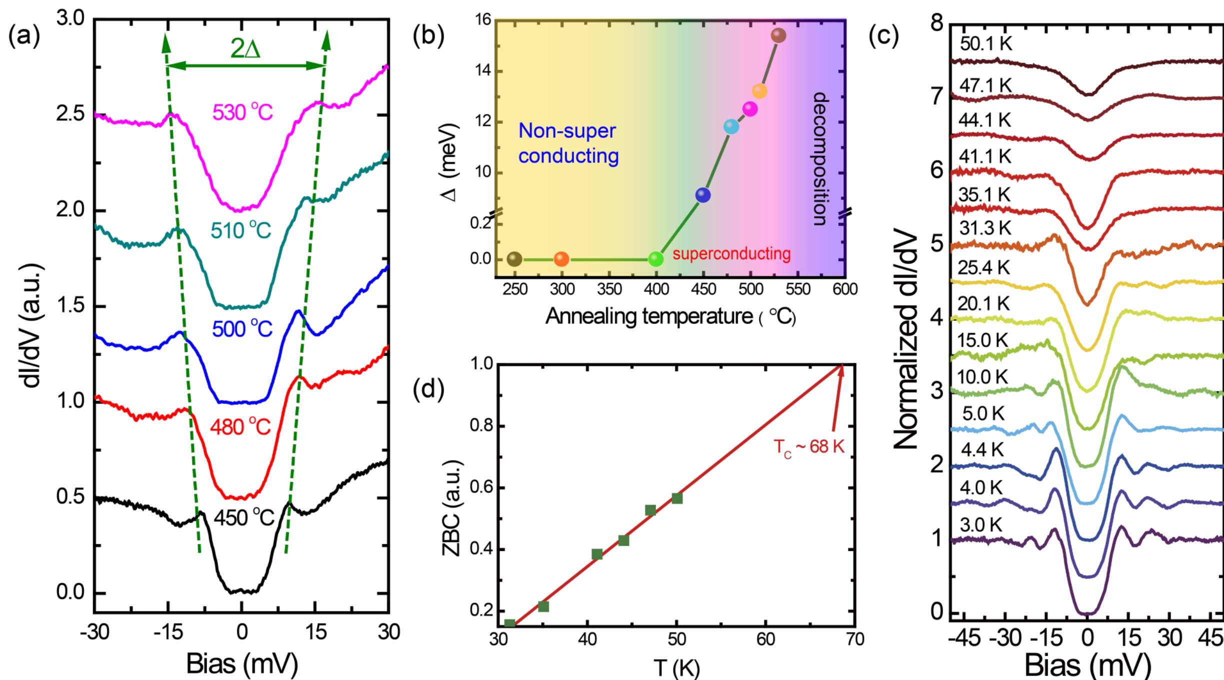

FIG. 2. (Color online) (a) The dI/dV spectra taken after annealing at 450, 480, 500, 510, and 530 °C. The corresponding gaps are 9.1, 11.8, 12.5, 13.2, and 15.4 meV, respectively. (b) The dependence of the superconducting gap with annealing temperature. (c) A series of normalized dI/dV spectra taken at various temperatures after annealing the 1-uc FeSe films at 530 °C. (d) The temperature dependence of ZBC extracted from the dI/dV spectra in (c). The spectra in (a) and (c) are shifted along the y axis at a fixed value of 0.5.

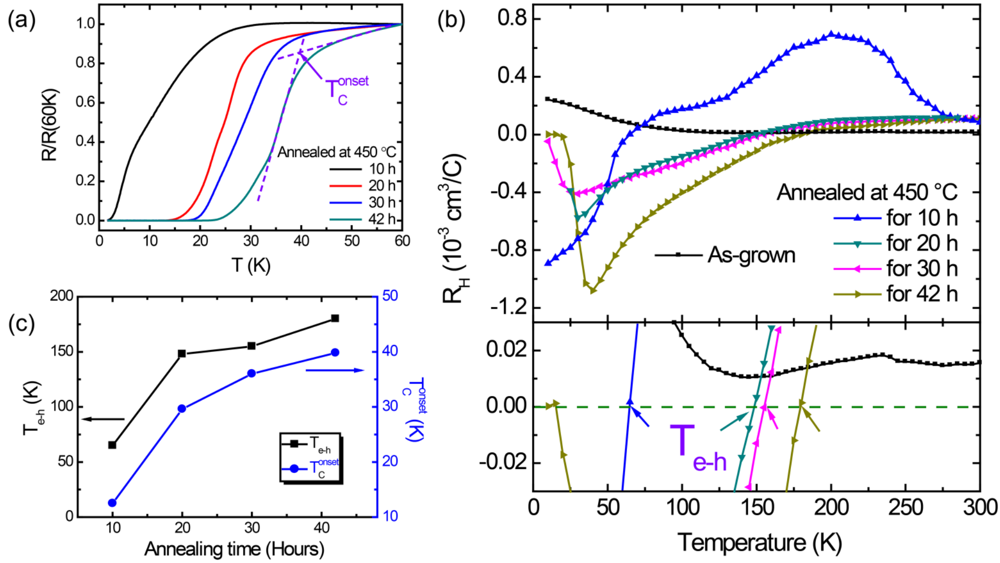

FIG. 3. (Color online) (a) $R(T)$ curves normalized at 60 K for 1-uc FeSe films annealed at 450 °C at various times. T_C^{onset} is defined as the dashed lines. (b) The temperature dependence of the Hall coefficient for as-grown films, as well as that annealed at 450 °C for different times. The bottom panel corresponds to the zoom-in region near $R_H = 0$, showing the change in carriers from hole type to electron type at $T_{e\text{-}h}$, indicated by the arrows. (c) T_C^{onset} and $T_{e\text{-}h}$, extracted from (a) and (b), respectively, plotted as a function of annealing time.

and a strong temperature-dependent behavior. R_H in all films is positive at 300 K, and decreases at lower temperature. In the case of semiconducting as-grown films, R_H remains positive: It reaches a minimum at ∼145 K and then increases again with decreasing temperature. The R_H of annealed superconducting films persists decreasing at lower temperature and changes to negative in the normal state before the superconducting transition, indicating a predominance of electron-type carriers, in contrast to the nonsuperconducting ones. The amplified-scale panel reveals a detailed change in sign from $R_H > 0$ to $R_H < 0$ at a characteristic temperature T_{e-h}. A very similar sign change has been reported in bulk iron chalcogenides [21], as well as in other superconductors [22], and is usually interpreted by the multiband feature of the electronic structure and the coexistence of electron and hole carriers with different contributions from various bands. Figure 3(c) summarizes the extracted T_C^{onset} and $T_{e\text{-}h}$ for the annealing time dependence. It is obvious that $T_{e\text{-}h}$ increases by prolonging the annealing time. The fact that both $T_{e\text{-}h}$ and T_C^{onset} increase with annealing time indicates a close relationship between superconductivity and charge carriers. Since a longer annealing time will lead to larger electron doping and will shift the E_F upwards, as seen by ARPES [7], more electrons are expected to participate in the transport process. Correspondingly, the sign reversal of R_H appears earlier, then the higher value of $T_{e\text{-}h}$. The results suggest that 1-uc FeSe films dominated by electron-type carriers are in favor of the superconducting transition.

The above transport results imply that electron doping plays an important role in the high-T_C superconductivity in 1-uc FeSe films. This is further supported by the result that T_C increases when electrons are injected into the 1-uc FeSe films by the field effect. The insulating STO substrate was used directly as a back gate, due to its high dielectric constant at low temperature [23–25]. Figure 4(a) shows the $R(T)$ curves of a 1-uc FeSe film (annealed at 450 °C for 30 h) under gate voltages (V_G) ranging from −200 to +200 V. The T_C^{onset} and normal resistance (R_n) at various gate voltages are summarized in Figs. 4(b) and 4(c), respectively. Clearly, the superconducting transition shifts to a lower temperature at negative voltages while it shifts to a higher temperature at positive bias. The T_C^{onset} is enhanced by ∼1.8 K at $V_G = +200$ V and suppressed by ∼5.6 K at $V_G = -200$ V. Applying positive voltage to the STO substrate corresponds to injecting extra electrons into the FeSe films, consequently leading to a decrease in the normal-state resistance, as well as to a shift of T_C^{onset} to a higher value. This indicates that electron doping indeed contributes to the interfacial superconductivity in the 1-uc FeSe films on STO substrates.

Finally, we discuss the possible origin of electron doping into the 1-uc FeSe films. Our STM and STS study has shown that the superconducting gap occurs with the formation of stoichiometric FeSe films and becomes larger with further

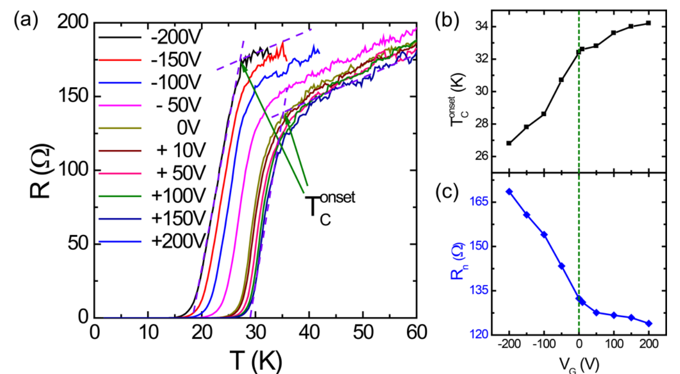

FIG. 4. (Color online) Field effect of the superconductivity in 1-uc FeSe films. (a) The $R(T)$ curves at various gate voltages. (b) The superconducting critical temperature and (c) normal resistance before the superconducting transition plotted as a function of gate voltage.

annealing, accompanied by an occurrence of Se vacancies. However, as seen in Fig. 1(h), the superconducting gap size on the isolated Se vacancy is just the same as that on the well-ordered region of stoichiometric FeSe, indicating that the existence of Se vacancies may not be the main origin of electron doping, even though the Se vacancies are expected to electrically dope the FeSe plane strongly [12].

We have observed a similar superconducting gap (Δ) and transition temperature (T_C) for the 1-uc FeSe films grown on insulating STO and on conductive Nb-STO substrates [4,13], consistent with previous ARPES studies of 1-uc films on conductive Nb-STO substrates [7,8]. The pretreatments of STO, namely, annealing at 950 °C for conductive Nb-STO and at 600 °C for insulating STO in an UHV condition, induces 2DEG at the STO surface [14,26]. This has been attributed to the localized oxygen vacancies at the surface and verified to be independent of the STO bulk properties over a large range of carrier densities from less than 10^{13} cm^{-3} (intrinsic insulating STO) to 10^{20} cm^{-3} (very conductive STO) [27]. Considering the similarity of such a bulk-independent feature, we attribute the main origin of electron doping to 2DEG or oxygen vacancies at the surface. This statement is consistent with previous first-principles calculations which stated that the oxygen deficiencies on the top layer of STO substrate can enhance the binding energy at the interface and can serve as the source of electron doping, leading to an increase in the local density of states at E_F [28–30]. We suggest that the substantial charge transfer and the charge-induced vertical electric field at the FeSe/STO interface should be responsible for the modified band structure and Fermi surface topology [7]. As a prerequisite, the FeSe films must be stoichiometric [31]. Otherwise, FeSe films with extra Se adatoms will experience hole doping [32], which may partially or even totally counteract the electron doping at the FeSe/STO interface. Postannealing treatments can remove extra Se adatoms and meanwhile keep the FeSe film stoichiometric so that the hole doping effect can be avoided.

In summary, we investigated the evolution of surface morphology, the superconducting gap, the superconducting transition temperature T_C, and charge carriers of 1-uc FeSe films on insulating STO substrates by a systematic annealing experiment. Our work reveals that the high-temperature superconductivity in the 1-uc FeSe/STO system is an interface effect and is caused by electron doping.

The work was financially supported by Ministry of Science and Technology and National Science Foundation of China. All STM topographic images were processed by WSxM software (www.nanotec.es).

[1] F.-C. Hsu, J.-Y. Luo, K.-W. Yeh, T.-K. Chen, T.-W. Huang, P. M. Wu, Y.-C. Lee, Y.-L. Huang, Y.-Y. Chu, D.-C. Yan, and M.-K. Wu, Proc. Natl. Acad. Sci. USA **105**, 14262 (2008).

[2] C.-L. Song, Y.-L. Wang, P. Cheng, Y.-P. Jiang, W. Li, T. Zhang, Z. Li, K. He, L. Wang, J.-F. Jia, H.-H. Hung, C. Wu, X. Ma, X. Chen, and Q.-K. Xue, Science **332**, 1410 (2011).

[3] E. Dagotto, Rev. Mod. Phys. **85**, 849 (2013).

[4] Q.-Y. Wang, Z. Li, W.-H. Zhang, Z.-C. Zhang, J.-S. Zhang, W. Li, H. Ding, Y.-B. Ou, P. Deng, K. Chang, J. Wen, C.-L. Song, K. He, J.-F. Jia, S.-H. Ji, Y.-Y. Wang, L.-L. Wang, X. Chen, X.-C. Ma, and Q.-K. Xue, Chin. Phys. Lett. **29**, 037402 (2012).

[5] S. Borisenko, Nat. Mater. **12**, 600 (2013).

[6] D. Liu, W. Zhang, D. Mou, J. He, Y.-B. Ou, Q.-Y. Wang, Z. Li, L. Wang, L. Zhao, S. He, Y. Peng, X. Liu, C. Chen, L. Yu, G. Liu, X. Dong, J. Zhang, C. Chen, Z. Xu, J. Hu, X. Chen, X. Ma, Q. Xue, and X. J. Zhou, Nat. Commun. **3**, 931 (2012).

[7] S. L. He, J. F. He, W. H. Zhang, L. Zhao, D. F. Liu, X. Liu, D. X. Mou, Y. B. Ou, Q. Y. Wang, Z. Li, L. L. Wang, Y. Y. Peng, Y. Liu, C. Y. Chen, L. Yu, G. D. Liu, X. L. Dong, J. Zhang, C. T. Chen, Z. Y. Xu, X. Chen, X. C. Ma, Q. K. Xue, and X. J. Zhou, Nat. Mater. **12**, 605 (2013).

[8] S. Tan, Y. Zhang, M. Xia, Z. R. Ye, F. Chen, X. Xie, R. Peng, D. F. Xu, Q. Fan, H. C. Xu, J. Jiang, T. Zhang, X. C. Lai, T. Xiang, J. P. Hu, B. P. Xie, and D. L. Feng, Nat. Mater. **12**, 634 (2013).

[9] K. Liu, Z.-Y. Lu, and T. Xiang, Phys. Rev. B **85**, 235123 (2012).

[10] Y.-Y. Xiang, F. Wang, D. Wang, Q.-H. Wang, and D.-H. Lee, Phys. Rev. B **86**, 134508 (2012).

[11] J. Bang, Z. Li, Y. Y. Sun, A. Samanta, Y. Y. Zhang, W. Zhang, L. Wang, X. Chen, X. Ma, Q.-K. Xue, and S. B. Zhang, Phys. Rev. B **87**, 220503(R) (2013).

[12] T. Berlijn, H.-P. Cheng, P. J. Hirschfeld, and W. Ku, Phys. Rev. B **89**, 020501(R) (2014).

[13] W.-H. Zhang, Y. Sun, J.-S. Zhang, F.-S. Li, M.-H. Guo, Y.-F. Zhao, H.-M. Zhang, J.-P. Peng, Y. Xing, H.-C. Wang, T. Fujita, A. Hirata, Z. Li, H. Ding, C.-J. Tang, M. Wang, Q.-Y. Wang, K. He, S.-H. Ji, X. Chen, J.-F. Wang, Z.-C. Xia, L. Li, Y.-Y. Wang, J. Wang, L.-L. Wang, M.-W. Chen, Q.-K. Xue, and X.-C. Ma, Chin. Phys. Lett. **31**, 017401 (2014).

[14] R. Di Capua, M. Radovic, G. M. De Luca, I. Maggio-Aprile, F. Miletto Granozio, N. C. Plumb, Z. Ristic, U. Scottidi Uccio, R. Vaglio, and M. Salluzzo, Phys. Rev. B **86**, 155425 (2012).

[15] M. J. Wang, J. Y. Luo, T. W. Huang, H. H. Chang, T. K. Chen, F. C. Hsu, C. T. Wu, P. M. Wu, A. M. Chang, and M. K. Wu, Phys. Rev. Lett. **103**, 117002 (2009).

[16] N. Li, Z. Li, H. Ding, S. Ji, X. Chen, and Q.-K. Xue, Appl. Phys. Express **6**, 113101 (2013).

[17] C. L. Song, Y. Yin, M. Zech, T. Williams, M. M. Yee, G.-F. Chen, J. L. Luo, N. L. Wang, E. W. Hudson, and J. E. Hoffman, Phys. Rev. B **87**, 214519 (2013).

[18] C.-L. Song, Y.-L. Wang, Y.-P. Jiang, Z. Li, L. Wang, K. He, X. Chen, X.-C. Ma, and Q.-K. Xue, Phys. Rev. B **84**, 020503 (2011).

[19] C. Y. Moon and H. J. Choi, Phys. Rev. Lett. **104**, 057003 (2010).

[20] C.-L. Song, Y.-L. Wang, Y.-P. Jiang, L. Wang, K. He, X. Chen, J. E. Hoffman, X.-C. Ma, and Q.-K. Xue, Phys. Rev. Lett. **109**, 137004 (2012).

[21] T. J. Liu, X. Ke, B. Qian, J. Hu, D. Fobes, E. K. Vehstedt, H. Pham, J. H. Yang, M. H. Fang, L. Spinu, P. Schiffer, Y. Liu, and Z. Q. Mao, Phys. Rev. B **80**, 174509 (2009).

[22] D. LeBoeuf, N. Doiron-Leyraud, J. Levallois, R. Daou, J.-B. Bonnemaison, N. E. Hussey, L. Balicas, B. J. Ramshaw,

R. Liang, D. A. Bonn, W. N. Hardy, S. Adachi, C. Proust, and L. Taillefer, Nature (London) **450**, 533 (2007).

[23] S. Thiel, G. Hammer, A. Schmeh, C. W. Schneider, and J. Mannhart, Science **313**, 1942 (2006).

[24] C. Bell, S. Harashima, Y. Kozuka, M. Kim, B. G. Kim, Y. Hikita, and H. Y. Hwang, Phys. Rev. Lett. **103**, 226802 (2009).

[25] J. Garcia-Barriocanal, A. Kobrinskii, X. Leng, J. Kinney, B. Yang, S. Snyder, and A. M. Goldman, Phys. Rev. B **87**, 024509 (2013).

[26] W. Meevasana, P. D. C. King, R. H. He, S.-K. Mo, M. Hashimoto, A. Tamai, P. Songsiriritthigul, F. Baumberger, and Z.-X. Shen, Nat. Mater. **10**, 114 (2011).

[27] A. F. Santander-Syro, O. Copie, T. Kondo, F. Fortuna, S. Pailhès, R. Weht, X. G. Qiu, F. Bertran, A. Nicolaou, A. Taleb-Ibrahimi, P. Le Fèvre, G. Herranz, M. Bibes, N. Reyren, Y. Apertet, P. Lecoeur, A. Barthélémy, and M. J. Rozenberg, Nature (London) **469**, 189 (2011).

[28] T. Bazhirov and M. L. Cohen, J. Phys.: Condens. Matter **25**, 105506 (2013).

[29] F. Yang, F. Wang, and D.-H. Lee, Phys. Rev. B **88**, 100504(R) (2013).

[30] F. Zheng, Z. Wang, W. Kang, and P. Zhang, Sci. Rep. **3**, 2213 (2013).

[31] T. M. McQueen, Q. Huang, V. Ksenofontov, C. Felser, Q. Xu, H. Zandbergen, Y. S. Hor, J. Allred, A. J. Williams, D. Qu, J. Checkelsky, N. P. Ong, and R. J. Cava, Phys. Rev. B **79**, 014522 (2009).

[32] Y. Chen, N. Pryds, J. E. Kleibeuker, G. Koster, J. Sun, E. Stamate, B. Shen, G. Rijnders, and S. Linderoth, Nano Lett. **11**, 3774 (2011).